Empirical Insights into Backward Directivity Estimation of CPW-Fed Flexible Antennas Using Characteristic Mode Analysis

Bashar Bahaa Qas Elias
Department of Information and Communication Engineering, College of Information Engineering, Al-Nahrain University, Jadriya, Baghdad, Iraq

Corresponding author: Bashar B. Qas Elias (e-mail: bashar.bahaa@nahrainuniv.edu.iq).

ABSTRACT This research proposes an empirical approach for estimating the backward directivity of a coplanar waveguide (CPW) flexible patch antenna using characteristic mode analysis (CMA). The proposed methodology involves developing a simple formula to calculate substrate-independent antenna backward directivity from the antenna's characteristic modes (CMs). It establishes a relationship between the characteristic modes and the antenna structure's natural resonant frequency, accounting for resonant frequency variations caused by substrate property changes. The approach remains valid for both traditional and complex antenna designs. Calculation results showed satisfactory agreement with simulation results, achieved without considering substrate or excitation effects. Finally, the approach demonstrated low error rates and rapid backward directivity. The method is verified with four antennas whose bandwidths range from 2 GHz to more than 11 GHz. Results illustrate that the estimation approach for conventional design attains a low rate of error (RoE) of 0.044.

INDEX TERMS backward directivity, CMA, flexible antenna, resonant frequency.

I. INTRODUCTION

ONE of the most essential components of a wireless communication system is the antenna [1], [2]. Depending on the frequency, its structure often occupies the most space in these systems. Other key factors considered during the design process include size, weight, cost, performance, manufacturing complexity, and the ability to support multiple frequency operations [3], [4]. Techniques to improve the antenna performance regarding gain and reduced back radiation are among the most researched topics [5], [6]. Wearable antennas typically enable wireless communication in electronic devices. Made of flexible materials, they can be seamlessly integrated into clothing and worn on the head, wrist, chest, or other body parts. Due to their adaptability, flexible antennas have been developed over the past decade using various materials, including electro-textiles. Such antennas are used for applications like indoor heart rate monitoring [8] and remote sensing for diabetic patients [7]. Additionally, the low dielectric constant of flexible materials like textiles can enhance antenna bandwidth and reduce surface wave losses [9]. Characteristic modes represent a set of orthogonal real currents on a conducting body's surface. These modes are independent of excitation and depend solely on the structure's size and shape [10]. While many computational electromagnetic solvers have increased flexibility in antenna design, Characteristic Mode Analysis (CMA) is unique because it determines a structure's electromagnetic properties without requiring excitation source. By solving the equivalent eigenmodes, the structure's bandwidth can be estimated more accurately and efficiently. Since the analysis results are excitation-independent, CMA provides a general electromagnetic solution for the structure [11]. This feature makes CMA particularly valuable, as it can identify the characteristic modes of any perfectly conducting structure.

In microstrip antennas, backward directivity occurs when electromagnetic waves are emitted opposite the main radiation lobe. This phenomenon can degrade antenna performance by increasing the front-to-back ratio (FBR), causing interference, and raising power loss. Recent studies have explored various strategies to mitigate backward directivity and enhance antenna efficiency [12]. Detecting and reducing backward directivity is crucial for optimizing performance. Engineers use precise detection methods, such as anechoic chambers with specialized equipment, to measure radiation patterns in all directions. The rear lobe levels in these patterns indicate the extent of backward directivity. Several techniques have been investigated to reduce back radiation, including:

i. Integrating metamaterial superstrates to suppress surface waves, thereby decreasing back radiation [13].

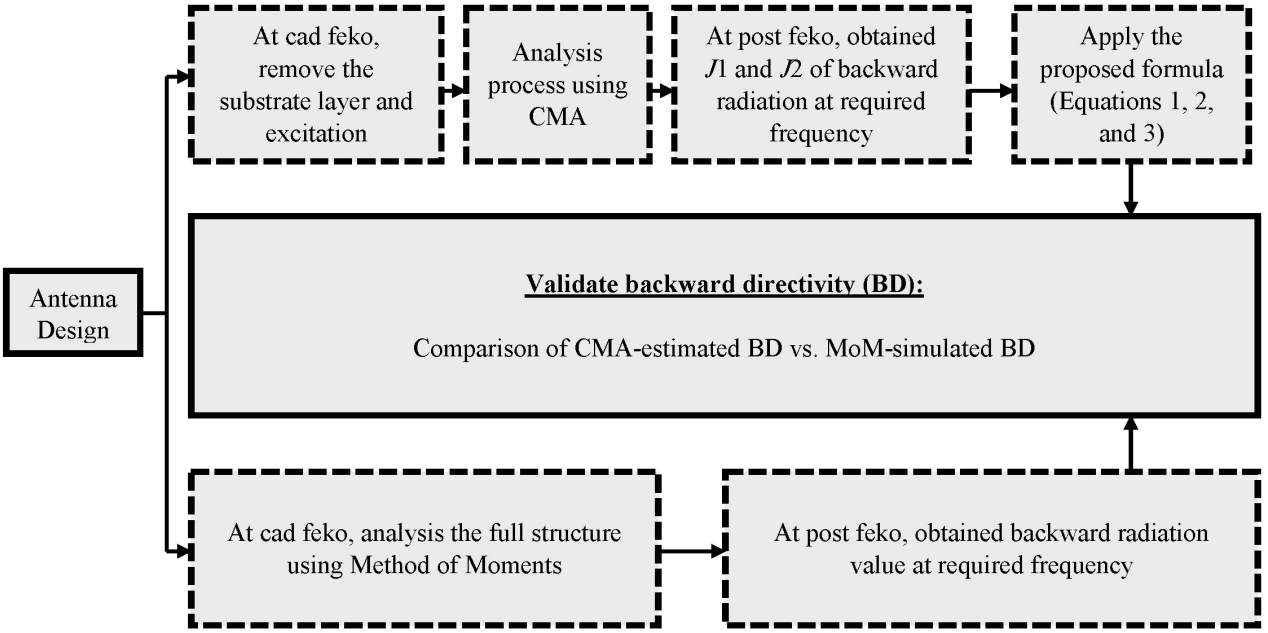

FIGURE 1. Summary of the proposed approach methodology.

ii. Employing frequency-selective surface (FSS)-based absorbing layers between the microstrip antenna and ground plane to control radiation characteristics and reduce back lobe levels [14].

This paper calculates an antenna's backward directivity using an estimated formula derived from the relationship between the structure's natural resonant frequency and its characteristic modes. **Figure 1** illustrates the proposed methodology. However, the method's application is currently limited to CPW flexible antennas due to CMA's substrate- and excitation-independent analysis. Future research incorporating diverse antenna structures and substrate materials is expected to expand this technique's applicability. The FEKO simulator was used for the antenna's design and analysis. To validate the efficiency of the proposed empirical approach, four wearable antenna designs are employed, as follows:

i. Design #1: a conventional elliptical patch antenna (CEPA).
ii. Design #2: a conventional rectangular patch antenna (CRPA).
iii. Design #3: a cloud-shaped patch antenna (CSPA).
iv. Design #4: a wideband patch antenna (WBPA).

Although the considered methodology provides a fast estimate of backward directivity, it should be stated that this technique is a semi-empirical design aid. It is meant to give antenna engineers a first-order approximation in the initial stages of design, thus avoiding the long computational times associated with full-wave optimization. All the simulation and calculation results based on the Method of Moments (MoM) and the CMA are illustrated in detail in the next sections of this work.

II. PROPOSED APPROACH– BASED CMA: OVERVIEW

The proposed approach based on CMA can be considered as an essential optimization strategy for ease of prediction of the antenna performance. To perform this approach, the following summarized steps can be carried out.

i. Firstly, the simplified radiator configuration is considered in absence of the substrate and excitations.
ii. The dominant modes ($J1$ and $J2$) at the target frequency are determined through CMA analysis of this structure. This can be determined by observing the total E-field magnitude (in volts) of the backward directivity of the antenna at 180°.
iii. Next, the proposed formula is employed to predict the backward directivity of the antenna. This formula is based on the magnitude of the voltage source and the E-field magnitude of the dominant modes, as demonstrated in **equations (1), (2), and (3)**.

$$S = \sqrt{ECR} \tag{1}$$

$$\text{Backward Directivity (BD)} = R \pm S \tag{2}$$

$$R = \frac{V_s \ (\text{in volt})}{0.1 \ . \ \overline{E_J} \ (\text{in volt})} \quad (3)$$

Where Vs is the magnitude of the voltage source (which was set to 1 V for all the models), and makes the radiation pattern results independent of absolute voltage scaling, and $\overline{Ej}$ is the average E-field magnitude [V] of the two dominant characteristic modes (J_1 and J_2) across all backward directivity angle (θ = 180°) in particular based on their evaluation in the backward direction. The factor of 0.1 in **Equation (3)** is the scaling factor that is found empirically relating the modal E-field magnitude to the normalized input voltage for the particular class of flexible CPW-fed antennas considered.

ECR indicates the error correction rate, varying depending on the antenna structure and ranging between (0 to 0.5). Since FEKO normalizes the radiation patterns based on relative power distribution, the directivity (both forward and backward) is usually independent of the absolute voltage value. However, if voltage variations alter the antenna current distribution or impedance matching, the backward directivity pattern could be affected. For this, the magnitude of the voltage source is supposed to be 1 volt in all cases of the antenna structures. The E-field strength is expressed in volts [V] after being normalized to a virtual sphere with a radius of one meter. This aims to eliminate the dependence of the far field on a factor of 1/distance (r), since field strength decreases with distance. This allows the FEKO simulator to display results independently of the observation distance. The change in units from [V/m] to [V] is due to multiplying the field value by the distance.

iv. Once the dominant modes are identified, the radiator is incorporated with its substrate and excitation. Here, the antenna is analyzed again, and the backward directivity obtained is compared with its calculated value from the proposed formula-based CMA.

Through the literature review, most researchers are dependent on optimization tools included in simulation software packages. These studies offer various approaches to estimate the backward directivity in patch antennas, contributing to advancements in antenna design and performance optimization. For example:

1. In contrast to a similar-sized metallic ground plane, the work in [15] demonstrated how to increase the FBR of a wideband patch antenna by 11.6 dB using a round, semitransparent ground plane with uniform impedance distribution. The idea is validated through simulations and experimental results, and the semitransparent ground plane is fabricated using an inexpensive carbon paste on a Kapton film.
2. The work in [16] proposed employing a capacitively loaded loop metamaterial superstrate (CLL-MTM) to reduce back radiation in microstrip patch antennas. The CLL-MTM superstrate effectively suppresses surface wave propagation, leading to a significant improvement in the FBR ratio with minimal impact on antenna gain and radiation efficiency.
3. To improve performance for off-body communication, the study in [17] designed a tri-band patch antenna with a perfectly conducting metal plate as a back reflector. By acting as a shield, the metallic plate improves directivity and reduces backward directivity while preventing frequency detuning caused by body proximity.

In contrast to the approaches described in the literature, the suggested approach is more straightforward and adaptable. This is due to simulations using the CMA-based approach not requiring the inclusion of the excitation or the substrate layer. As a result, antenna directivity can be estimated with less time and optimization effort, and the approach can be applied to various antenna structures with different levels of complexity. The next section explains four design examples that demonstrate the effectiveness and application of this approach. The choice of the ECR is heuristic and based on the deterministic changes in radiation patterns introduced by the metallic radiator when placed over a dielectric substrate with given dimensions and specific excitation. In practice, ECR of 0.1 to 0.2 is chosen for traditional designs to preserve maximum precision. Moreover, averaging the first two dominant modes (J_1 and J_2) at $\theta = 180°$ has a physical meaning since they represent the two main current distributions that render the fundamental resonance of the radiator.

III. ANTENNA DESIGN CONSIDERATIONS

A. DESIGN #1: CEPA

The first design allows for a single-layer radiator by implementing a conventional elliptical microstrip patch structure on a flexible Kapton polyimide substrate, fed by a CPW line. Careful impedance matching is essential for optimal performance, as the distance between the CPW and the feed line significantly affects it. **Figure 2** illustrates the elliptical patch geometry of this design.

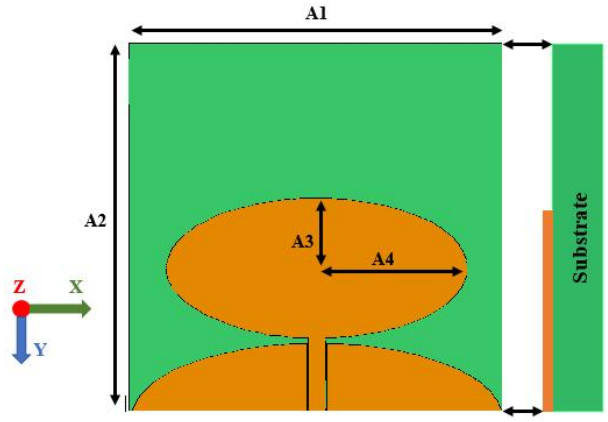

FIGURE 2. The layout of the CEPA.

B. DESIGN #2: CRPA

The subsequent antenna is fed by a CPW line and features a traditional rectangular design, as illustrated in **Figure 3**. The antenna's impedance matching depends on the space between the feed line and the CPW, which must be carefully optimized for proper resonance.

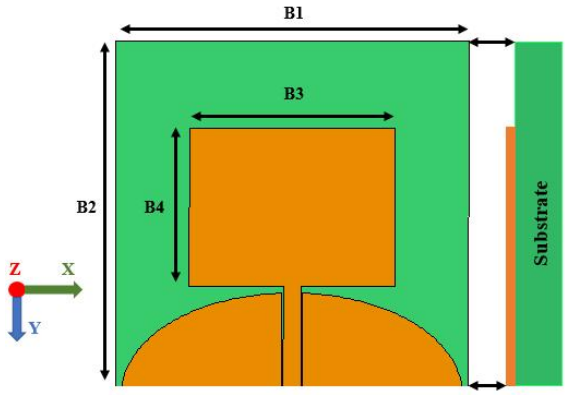

FIGURE 3. The layout of the CRPA.

C. DESIGN #3: CSPA

The cloud-shaped patch antenna is printed on Kapton polyimide using a substrate material similar to that of previous designs [18]. This flexible material offers stability during operation and ease of fabrication. Its properties include low moisture absorption, precise thickness control, mechanical stability, and a consistent dielectric constant. The fractal antenna's cloud shape consists of multiple elliptical elements with dimensions C_3 , C_4 , C_5 , and C_6 , as shown in **Figure 4**.

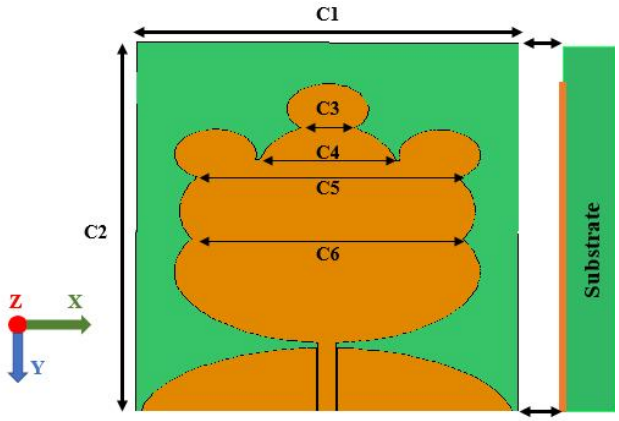

(a)

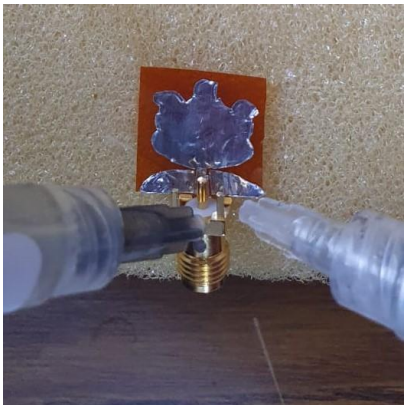

(b)

FIGURE 4 . The layout of the CSPA [18]: (a) simulated design (b) fabricated design.

D. DESIGN #4: WBPA

The topology for the compact wideband antenna is presented in this section [19]. As shown in **Figure 5**, the radiating patch consists of three main sections: a half-circle patch at the bottom, an ovoid patch in the middle, and a rectangular patch at the top. These sections are connected by two rectangular arms on the radiator's left and right edges. In this work, the CPW feeding technique is employed to minimize the quality factor (Q) and generate additional modes, resulting in multiband and wide-resonance behavior [20–25].

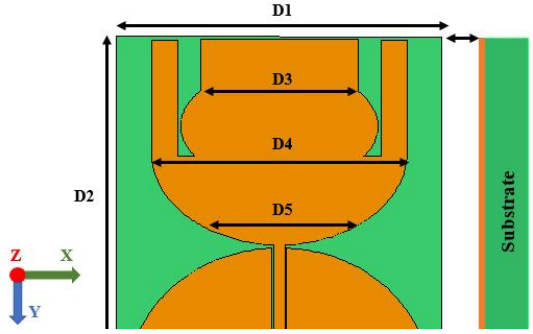

(a)

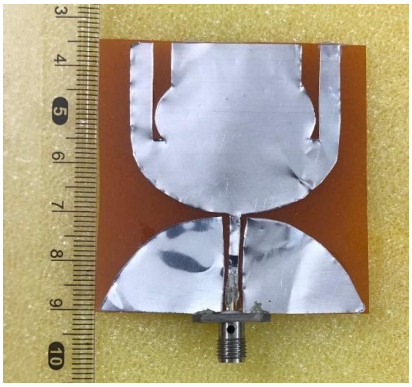

(b)

FIGURE 5. The layout of the WBPA [19]: (a) simulated design (b) fabricated design.

The overall parameters and dimensions for all designs presented in this study are listed in **Table 1**.

TABLE I. Overall dimensions of the antennas

Parameter	Value (mm)	Parameter	Value (mm)
A1	15	*C3*	2.12
A2	15	*C4*	5.51
A3	2.8	*C5*	10.24
A4	5.8	*C6*	10.65
B1	70	*D1*	56
B2	70	*D2*	56
B3	40.81	*D3*	27
B4	31.37	*D4*	44
C1	15	*D5*	28.89
C2	15	*h*	0.11
Relative permittivity (ε_r)	3.5	*Loss tangent* ($\tan\delta$)	0.045

IV. RESULTS AND OBSERVATIONS

A. DESIGN #1: CEPA

The radiation characteristics are analysed as the initial step using CMA, then the MoM is employed. According to **Figure 6**, the CEPA shows a 10-dB bandwidth of 4.68 GHz (from 13.17 to 17.84 GHz). Additionally, the modal significance (MS) analysis exhibits the dominant modes (1 and 2) of the radiator patch.

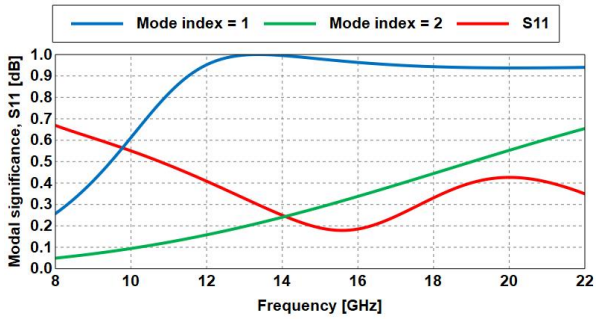

FIGURE 6. Simulation results of a CEPA: MS and reflection coefficient.

Next, the empirically proposed approach is applied to estimate the backward directivity of the antenna based on the CMA technique, as described in Section 2. **Figure 7** shows that the backward directivity of the antenna is obtained at $\theta = 180^{o}$. For example, at 13.37 GHz, which is one of the operating frequencies among the obtained band, at the first two dominant modes, the electric field has the magnitude values of 7.41 V and 8.30 V, respectively, as demonstrated in **Figure 7(a)**. The average value for these two modes is 7.85 V. On the other hand, the gain achieved is 1.67 in this θ direction when the analysis is performed on the full antenna structure as shown in **Figure 7(b)**. Next, the estimate of backward directivity can be determined based on the proposed formula defined in **Equation (2)**, as follows:

$$\text{Backward Directivity (BD)} = \left[\frac{V_s\ (\text{in volt})}{0.1\ (\overline{E_J}\ (\text{in volt}))}\right] + \sqrt{\text{ECR}}$$

$$\text{Backward Directivity (BD)} = \left[\frac{1}{0.1(\frac{7.41+8.3}{2})}\right] + \sqrt{0.2}$$

$$\text{Backward Directivity (BD)} = 1.72$$

Then, it is observed that the RoE between the backward directivity produced by the analysis of the complete antenna and the value obtained by the proposed formula is 0.044; this is due to the impact of the substrate material and the excitation of the antenna.

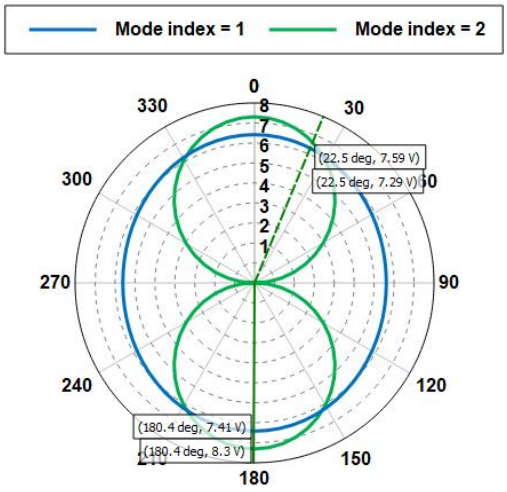

(a)

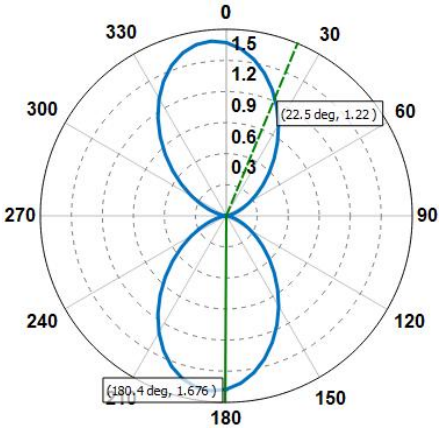

(b)

FIGURE 7. Backward directivity results of CEPA (a) analysis of the radiator using CMA (b) analysis of complete antenna using MoM.

B. DESIGN #2: CRPA

The simulation results in **Figure 8** displayed the full analysis of the proposed antenna in addition to the CMA analysis of the radiator. The bandwidth of approximately greater than 2 GHz is achieved; besides, the MS of the dominant modes is significantly observed.

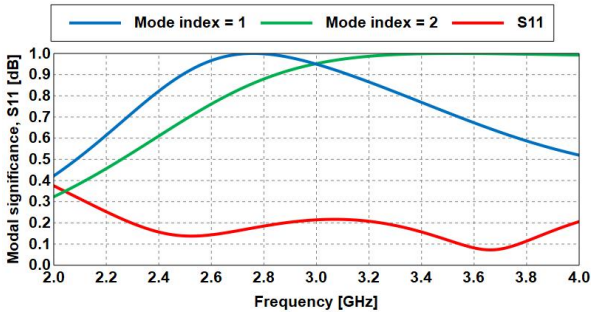

FIGURE 8 .Simulation results of a CRPA: MS and reflection coefficient.

Moreover, CMA analysis of a conventional rectangular radiator shows that the dominant modes (mode 1 and mode 2) at the frequency of 2.75 GHz are 7.49 and 7.47, respectively, as illustrated in **Figure 9(a)**. After that, the antenna is incorporated into the substrate. At excitation, it becomes evident that its backward directivity is equal to 1.94, as shown in **Figure 9(b)**. The estimate of backward directivity can be determined based on the proposed formula defined in **Equation (2),** as follows:

$$\text{Backward Directivity (BD)} = \left[\frac{V_s \ (\text{in volt})}{0.1\ (\overline{E_J}\ (\text{in volt}))}\right] + \sqrt{\text{ECR}}$$

$$\text{Backward Directivity (BD)} = \left[\frac{1}{0.1(\frac{7.49+7.47}{2})}\right] + \sqrt{0.2}$$

$$\text{Backward Directivity (BD)} = 1.78$$

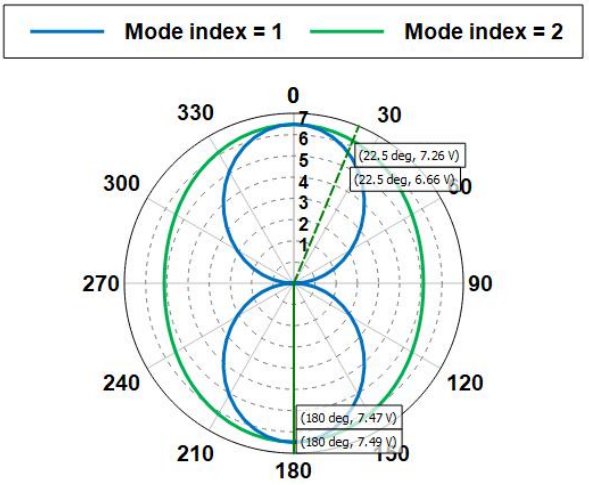

(a)

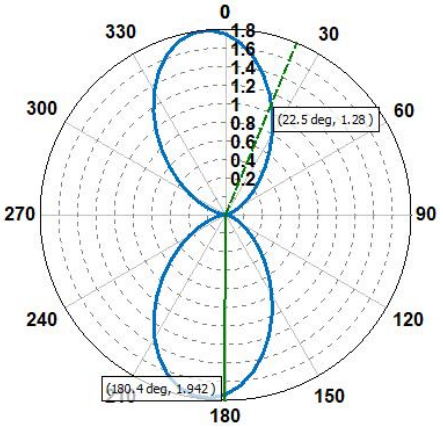

(b)

FIGURE 9. Backward directivity results of CRPA (a) analysis of the radiator using CMA (b) analysis of complete antenna using MoM.

Then, it is observed that the rate of error between the backward directivity produced by the analysis of the complete antenna and the value obtained by the proposed formula is 0.162.

C. DESIGN #3: CSPA

First, the characteristics of the CSPA radiation are evaluated using CMA and the MoM. Based on **Figure 10**, this antenna exhibits a 10-dB bandwidth of 11.28 GHz, covering a frequency range from 9.03 GHz to 20.31 GHz.

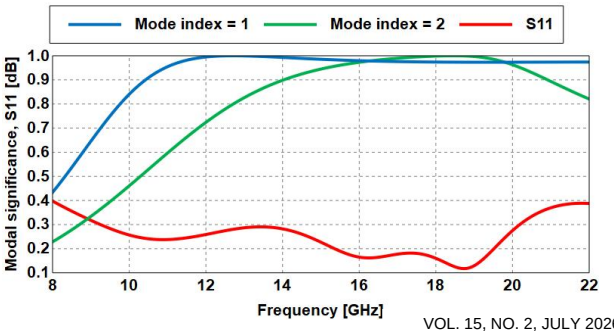

FIGURE 10. Simulation results of a CSPA: MS and reflection coefficient.

A key factor in determining the antenna's performance is the radiator patch's dominant modes (modes 1 and 2), which are highlighted by the MS analysis. Based on the CMA technique, the empirically suggested approach is used to estimate the antenna's backward directivity. **Figure 11** demonstrates that the antenna's backward directivity occurs at θ = 180°, proving the accuracy of the suggested estimation approach. For instance, **Figure 11(a)** shows that the electric field magnitude values at modes 1 and 2 are 7.86 V and 8.28 V, respectively, at 12.66 GHz—one of the operating frequencies within the obtained bandwidth. The average value for these two modes is calculated to be 8.07 V. On the other hand, as illustrated in **Figure 11(b)**, the gain obtained in this θ direction when examining the entire antenna structure is 1.78. The following formula defined in **Equation (2),** can be used to calculate the estimated backward directivity.

$$\text{Backward Directivity (BD)} = \left[\frac{V_s\ (\text{in volt})}{0.1\ (\overline{E_J}\ (\text{in volt}))}\right] + \sqrt{\text{ECR}}$$

$$\text{Backward Directivity (BD)} = \left[\frac{1}{0.1(\frac{7.86+8.28}{2})}\right] + \sqrt{0.2}$$

$$\text{Backward Directivity (BD)} = 1.69$$

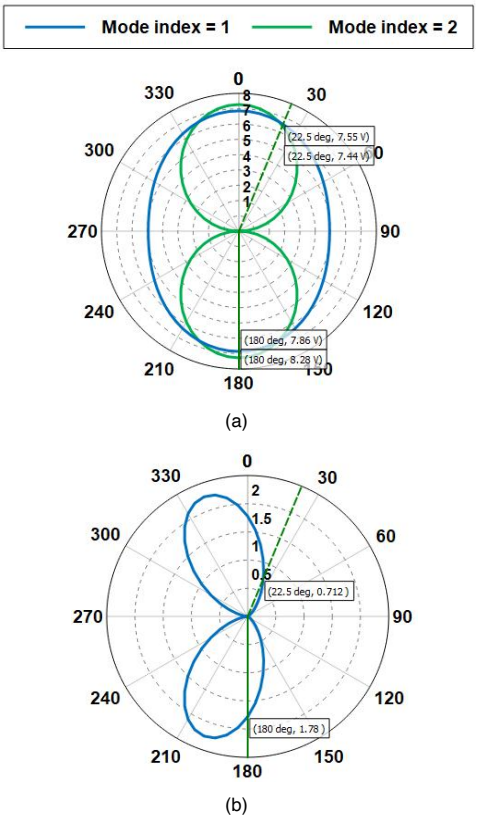

FIGURE 11 Backward directivity results of a CSPA (a) analysis of the radiator using CMA (b) analysis of complete antenna using MoM.

It is observed that the rate of error between the backward directivity derived from the full antenna analysis and the value obtained using the proposed formula is 0.09, indicating a high degree of accuracy in the estimation approach.

D. DESIGN #4: WBPA

In the final case study, the radiation properties of the wideband patch antenna are initially examined using CMA along with the MoM. According to **Figure 12**, this antenna demonstrates a 10-dB bandwidth exceeding 4 GHz.

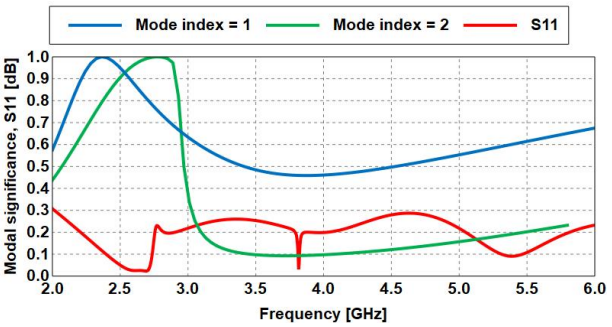

FIGURE 12. Simulation results of a WBPA: MS and reflection coefficient.

The analysis of MS identifies mode 1 and mode 2 as the primary resonant modes of the radiator patch, which significantly influence the antenna's overall performance. An empirically developed approach is utilized to estimate the backward directivity of the antenna design-based CMA approach methodology. As depicted in **Figure 13**, the backward directivity is observed at an angle of θ = 180°, validating the accuracy of the proposed estimation technique. For instance, at an operating frequency of 2.36 GHz, which falls within the identified bandwidth, the electric field magnitudes for the first two modes are recorded as 7.05 V and 7.43 V, respectively, as shown in **Figure 13(a)**. The computed average of these values is 7.24 V. Furthermore, when analyzing the complete antenna structure, the gain at this θ direction is determined to be 1.76, as illustrated in **Figure 13(b)**. The estimated backward directivity is obtained using the following proposed formula defined in **Equation (2)**:

$$\text{Backward Directivity (BD)} = \left[\frac{V_s\ (\text{in volt})}{0.1\ (\overline{E_J}\ (\text{in volt}))}\right] + \sqrt{\text{ECR}}$$

$$\text{Backward Directivity (BD)} = \left[\frac{1}{0.1(\frac{7.05+7.43}{2})}\right] + \sqrt{0.2}$$

$$\text{Backward Directivity (BD)} = 1.82$$

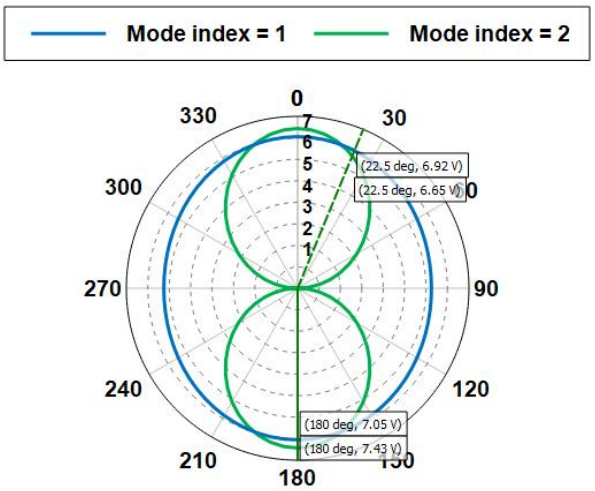

(a)

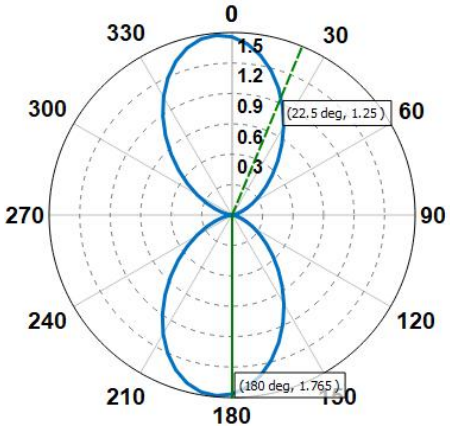

(b)

FIGURE 13. Backward directivity results of a WBPA (a) analysis of the radiator using CMA (b) analysis of complete antenna using MoM.

Additionally, the error margin between the backward directivity derived from the full antenna analysis and the estimated value using the formula is found to be 0.05, demonstrating a high level of precision in the proposed estimation approach.

Furthermore, different resonant frequencies of each design are evaluated based on the proposed formula at different ECR values (from 0.1 to 0.5) as shown in **Tables (II to VI)**.

TABLE II. Validation of the proposed formula at different frequencies of the designs at an ECR value of 0.1

Design	Frequency (GHz)	BD based proposed formula (unitless)	BD based simulation (unitless)	RoE (unitless)
CEPA	14	1.57	1.685	0.115
	15.6	1.529	1.668	0.139
	16	1.518	1.645	0.127
	17	1.492	1.518	0.026
	17.61	1.479	1.376	0.103
CRPA	2.5	1.671	1.839	0.168
	3	1.64	2.027	0.387
	3.4	1.657	2.046	0.389
	3.7	1.723	1.837	0.114
	3.8	1.756	1.689	0.067
CSPA	10.9	1.607	1.793	0.186
	13	1.543	1.738	0.195
	16	1.462	0.767	0.695
	18.73	1.518	0.679	0.839
	20	1.814	0.313	1.501
WBPA	2.67	1.684	1.983	0.299
	3.3	2.237	2.13	0.107
	3.82	2.31	1.931	0.379
	4.5	2.403	1.428	0.975
	5.4	2.403	0.904	1.499

TABLE III. Validation of the proposed formula at different frequencies of the designs at an ECR value of 0.2

Design	Frequency (GHz)	BD based proposed formula (unitless)	BD based simulation (unitless)	RoE (unitless)
CEPA	14	1.701	1.685	0.016
	15.6	1.66	1.668	0.008
	16	1.649	1.645	0.004
	17	1.623	1.518	0.105
	17.61	1.61	1.376	0.234
CRPA	2.5	1.802	1.839	0.037
	3	1.771	2.027	0.256
	3.4	1.788	2.046	0.258
	3.7	1.854	1.837	0.017
	3.8	1.887	1.689	0.198
CSPA	10.9	1.738	1.793	0.055
	13	1.674	1.738	0.064
	16	1.593	0.767	0.826
	18.73	1.649	0.679	0.97
	20	1.945	0.313	1.632
WBPA	2.67	1.815	1.983	0.168
	3.3	2.368	2.13	0.238
	3.82	2.445	1.931	0.514
	4.5	2.534	1.428	1.106
	5.4	2.534	0.904	1.63

TABLE IV. Validation of the proposed formula at different frequencies of the designs at an ECR value of 0.3

Design	Frequency (GHz)	BD based proposed formula (unitless)	BD based simulation (unitless)	RoE (unitless)
CEPA	14	1.801	1.685	0.116
	15.6	1.761	1.668	0.093
	16	1.749	1.645	0.104
	17	1.724	1.518	0.206
	17.61	1.71	1.376	0.334
CRPA	2.5	1.902	1.839	0.063
	3	1.872	2.027	0.155
	3.4	1.889	2.046	0.157
	3.7	1.955	1.837	0.118
	3.8	1.987	1.689	0.298
CSPA	10.9	1.838	1.793	0.045
	13	1.774	1.738	0.036
	16	1.693	0.767	0.926
	18.73	1.75	0.679	1.071
	20	2.045	0.313	1.732
WBPA	2.67	1.915	1.983	0.068
	3.3	2.468	2.13	0.338
	3.82	2.545	1.931	0.614
	4.5	2.635	1.428	1.207
	5.4	2.635	0.904	1.731

TABLE V. Validation of the proposed formula at different frequencies of the designs at an ECR value of 0.4

Design	Frequency (GHz)	BD based proposed formula (unitless)	BD based simulation (unitless)	RoE (unitless)
	14	1.886	1.685	0.201
	15.6	1.846	1.668	0.178
CEPA	16	1.834	1.645	0.189
	17	1.808	1.518	0.29
	17.61	1.795	1.376	0.419
	2.5	1.987	1.839	0.148
	3	1.956	2.027	0.071
CRPA	3.4	1.973	2.046	0.073
	3.7	2.039	1.837	0.202
	3.8	2.072	1.689	0.383
	10.9	1.923	1.793	0.13
	13	1.859	1.738	0.121
CSPA	16	1.778	0.767	1.011
	18.73	1.835	0.679	1.156
	20	2.13	0.313	1.817
	2.67	2	1.983	0.017
	3.3	2.553	2.13	0.423
WBPA	3.82	2.63	1.931	0.699
	4.5	2.72	1.428	1.292
	5.4	2.72	0.904	1.816

TABLE VI. Validation of the proposed formula at different frequencies of the designs at an ECR value of 0.5

Design	Frequency (GHz)	BD based proposed formula (unitless)	BD based simulation (unitless)	RoE (unitless)
	14	1.961	1.685	0.276
	15.6	1.92	1.668	0.252
CEPA	16	1.909	1.645	0.264
	17	1.883	1.518	0.365
	17.61	1.869	1.376	0.493
	2.5	2.062	1.839	0.223
	3	2.031	2.027	0.004
CRPA	3.4	2.048	2.046	0.002
	3.7	2.114	1.837	0.277
	3.8	2.146	1.689	0.457
	10.9	1.998	1.793	0.205
	13	1.934	1.738	0.196
CSPA	16	1.853	0.767	1.086
	18.73	1.909	0.679	1.23
	20	2.205	0.313	1.892
	2.67	2.07	1.983	0.087
	3.3	2.628	2.13	0.498
WBPA	3.82	2.705	1.931	0.774
	4.5	2.794	1.428	1.366
	5.4	2.794	0.904	1.89

In light of the obtained results, it is evident that the average of RoE in the case of conventional antennas (CEPA and CRPA) is significantly lower than that in the case of antennas with complex structures (CSPA and WBPA), as shown in **Table 7** and **Figure 14**. The RoE value is also observed to increase at higher frequencies. In these two cases, it is recommended to use the formula (BD=R-S) in the case of higher frequencies and traditional antennas to keep the value of RoE to a minimum. Finally, it is important to emphasize that the proposed approach is an empirical formula that can be used by antenna engineers to predict the backward directivity of the antennas in a relatively short period.

TABLE VII. Summation of RoE of the designs at different ECR values

Design	0.1 ECR	0.2 ECR	0.3 ECR	0.4 ECR	0.5 ECR
CEPA	0.51	0.367	0.853	1.277	1.65
CRPA	1.125	0.766	0.791	0.877	0.963
CSPA	3.416	3.547	3.81	4.235	4.609
WBPA	3.259	3.656	3.958	4.247	4.615

FIGURE 14. Summation of RoE of the designs at different ECR values.

It can be seen that the error increases when the method is used for complex geometries (CSPA and WBPA) or at high frequencies. This is due to the fact that higher-order modes are more dominant, but these modes are not included in the dominant-mode averaging. Therefore, for ordinary planar radiators in the principal resonance bands, where minimum values of RoE are encountered, a firm definition of the admissible range of the method can be most reliably obtained.

V. CONCLUSION

This study employs CMA to analyze the backward directivity of a Flexible CPW patch antenna in an efficient manner. The method provides a useful relationship between characteristic modes and the natural resonant frequency of the antenna, considering (through a derived substrate-independent expression) the substrate parameter variations. The effectiveness of the method is verified for both conventional and slotted antennas with very good results. The low-error method ensures the trustworthiness of the results. Using this approach, an antenna designer can predict the backward directivity either more swiftly or more accurately. The validation of the proposed method is at present only via a high-fidelity benchmark based on MoM simulations. While these results suggest that the theoretical application of the formula based on the CMA is feasible, further works will focus on the experimental validation in anechoic chambers to verify the performance of the proposed method in a real testing scenario.

REFERENCES

[1] R. Joshi and A. Sharma, "Compact size and high gain microstrip patch antenna design for mmWave 5G wireless communication," in Proc. 2024 Int. Conf. Integr. Circuits Commun. Syst. (ICICACS), Raichur, India, 2024, pp. 1–4, DOI: 10.1109/ICICACS60521.2024.10498315.

[2] B. Q. Elias, M. Alsajri, P. J. Soh, and A. A. Al-Hadi, "Design of flexible planar antennas using substrate gap structure for surface wave reduction," in Proc. 2019 22nd Int. Conf. Control Syst. Comput. Sci. (CSCS), Bucharest, Romania, 2019, pp. 453–458, DOI: 10.1109/CSCS.2019.00083.

[3] H. Zhao, Q. Wang, J. Du, L. Chen, W. Yue, and W. Wang, "Micro-electromechanical system-based parasitic patch antenna on quartz substrate for high gain," Sensors, vol. 25, no. 3, p. 607, 2025, DOI: 10.3390/s25030607.

[4] Z. Siddiqui et al., "Dual-band dual-polarized planar antenna for 5G millimeter-wave antenna-in-package applications," IEEE Trans. Antennas Propag, vol. 71, no. 4, pp. 2908–2921, Apr. 2023, DOI: 10.1109/TAP.2023.3240032.

[5] M. Tamma, A. Boonjue, W. Wiboonjaroen, S. Ramphueiphad, and S. Kampeephat, "Performance improvement of slot antenna with metamaterial for modern wireless communication," Results Eng, vol. 23, p. 102686, 2024, DOI: 10.1016/j.rineng.2024.102686.

[6] A. S. Abdel Halim, Z. Abdel-Salam, M. Abdel-Harith, and O. Hamdy, "Investigating the effect of changing the substrate material analyzed by laser-induced breakdown spectroscopy on the antenna performance," Sci. Rep, vol. 14, no. 1, p. 1964, Jan. 2024, DOI: 10.1038/s41598-024-52435-3.

[7] X. Yang et al., "Freezing of gait detection considering leaky wave cable," IEEE Trans. Antennas Propag., vol. 67, pp. 554–561, 2019, DOI: 10.1109/TAP.2018.2878081.

[8] B. B. Q. Elias, A. A. Al-Hadi, P. Akkaraekthalin, and P. J. Soh, "A dimension estimation method for rigid and flexible planar antennas based on characteristic mode analysis," Electronics, vol. 11, no. 21, p. 3585, 2022, DOI: 10.3390/electronics11213585.

[9] N. Singh, V. Singh, R. Saini, J. P. Saini, and A. Bhoi, "Microstrip textile antenna with jeans substrate with applications in S-band," in Adv. Commun., Devices, Netw, Singapore: Springer, 2018, pp. 369–376, DOI: 10.1007/978-981-10-7901-6_40.

[10] C. Deng, Z. Zhao, and W. Yu, "Characteristic mode analysis of circular microstrip patch antenna and its application to pattern diversity design," IEEE Access, vol. 10, pp. 2399–2407, 2022, DOI: 10.1109/ACCESS.2021.3139316.

[11] M. Khan, T. Murad, and N. Lusdyk, "Beamforming analysis of dual beam antenna array using theory of characteristic modes," IEEE Open J. Antennas Propag, vol. 5, no. 6, pp. 1465–1475, Dec. 2024, DOI: 10.1109/OJAP.2024.3449752.

[12] J. Zhang, H. Shi, Z. Fan, T. Jiang, C. Ma, and S. Dong, "Design of a dual-polarized microstrip antenna with low backward radiation," in Proc. 2023 6th Int. Conf. Commun. Eng. Technol. (ICCET), Xi'an, China, 2023, pp. 89–93, DOI: 10.1109/ICCET58756.2023.00023.

[13] A. Jafargholi, A. Jafargholi, and J. H. Choi, "Mutual coupling reduction in an array of patch antennas using CLL metamaterial superstrate for MIMO applications," IEEE Trans. Antennas Propag, vol. 67, no. 1, pp. 179–189, Jan. 2019, DOI: 10.1109/TAP.2018.2874747.

[14] A. Raj and N. Gupta, "Radiation characteristics of microstrip antenna on frequency selective surface absorbing layer,"Int. J. Microw. Wireless Technol, vol. 13, no. 9, pp. 962–968, 2021, DOI: 10.1017/S1759078720001610.

[15] K. Klionovski and A. Shamim, "Back radiation suppression through a semitransparent ground plane for a mm-wave patch antenna," IEEE Trans. Antennas Propag, vol. 65, no. 8, pp. 3935–3941, 2017, DOI: 10.1109/TAP.2017.2717967.

[16] A. Jafargholi, A. Jafargholi, J. H. Choi, M. Veysi, and A. Soleimani, "Microstrip patch back radiation reduction using metamaterial superstrate," IET Microw. Antennas Propag, vol. 14, no. 2, pp. 158–164, Nov. 2019, DOI: 10.1049/iet-map.2018.6237.

[17] A. Gupta and V. Kumar, "Design of a tri-band patch antenna with back reflector for off-body communication," Wireless Pers. Commun, vol. 115, pp. 173–185, 2020, DOI: 10.1007/s11277-020-07566-x.

[18] B. B. Q. Elias, M. A. Alqaisy, and P. J. Soh, "Design of X/Ku and K band flexible cloud-fractal wideband antenna with bandwidth estimation using CMA," Microwave Rev, vol. 30, no. 1, pp. 23–28, 2024, DOI: 10.18485/mtts_mr.2024.30.1.4.

[19] B. B. Q. Elias and P. J. Soh, "Resonance analysis and gain estimation using CMA-based even mode combination method for flexible wideband antennas" Sensors, vol. 23, no. 11, p. 5297, June 2023.

[20] L.-M. Si and X. Lv, "CPW-fed multi-band omni-directional planar microstrip antenna using composite metamaterial resonator for wireless communications," Prog. Electromagn. Res, vol. 83, pp. 133–146, 2008, DOI: 10.2528/pier08050404.

[21] R. P. Dwivedi and U. K. Kommuri, "CPW feed dual band and wideband antennas using crescent shape and T-shape stub for Wi-Fi and WiMAX application,"Microw. Opt. Technol. Lett, vol. 59, pp. 2586–2591, 2017, DOI: 10.1002/mop.30786.

[22] W.-C. Liu, C.-M. Wu, and N.-C. Chu, "A compact CPW-fed slotted patch antenna for dual-band operation," IEEE Antennas Wirel. Propag. Lett, vol. 9, pp. 110–113, 2010, DOI: 10.1109/LAWP.2010.2044135.

[23] M. Hua, P. Wang, Y. Zheng, and S. Yuan, "Compact tri-band CPW-fed antenna for WLAN/WiMAX applications," Electron. Lett, vol. 49, pp. 1118–1119, 2013, DOI: 10.1049/el.2013.1669.

[24] W. A. Awan et al., "A miniaturized wideband and multi-band on-demand reconfigurable antenna for compact and portable devices," AEU - Int. J. Electron. Commun,, vol. 122, p. 153266, 2020, DOI: 10.1016/j.aeue.2020.153266.

[25] R. Wu, P. Wang, Q. Zheng, and R. Li, "Compact CPW-fed triple-band antenna for diversity applications" Electron. Lett, vol. 51, pp. 735–736, 2015, DOI: 10.1049/el.2015.0466.